Marker pen writing of perovskite solar modules

Yuhao Song[1,3], Miaosen Yao[1,3], Chen Dong ●[1] ✉, Sergey Dayneko ●[2], Gaogeng Wang[1], Dongyang Zhang[2], Yingying Deng[1], Junjie Tong[1], Qichao Wang[1], Gentian Yue[1], Yueyue Gao[1], Weifeng Zhang[1], Makhsud I. Saidaminov ●[2] ✉ & Furui Tan ●[1] ✉

Solution-processed perovskite photovoltaics promise low-cost, lightweight, and wearable power sources. Processing techniques play a crucial role in this field. Here, we introduce a large-area, patternable, and cyclable film writing technique that utilizes marker pen as a fabrication tool. By adjusting ink concentration, pressure, writing speed, tip width, solvent engineering, and using fiber-capillary structure of marker pens, we demonstrate control over perovskite ink colloids, film thickness (from 200 to > 1000 nm) and area (from 1 to 100+ cm^2) patterning on rigid and flexible substrates, as well as ambient writing of crystalline perovskite film. Marker pen written rigid and flexible carbon-electrode perovskite solar modules in mask- and laser-free manners achieve 16.3% and 14.5% power conversion efficiencies, respectively. This method offers an opportunity for rapid on-site fabrication of lightweight and deformable power sources on various substrates, including inflated elastic balloons and folded cellophane paper, and produces customizable irregular solar modules.

Thanks to their photoelectric properties, which include tunable bandgap, high light absorption coefficient, low exciton binding energy, and long charge carrier diffusion length, organic-inorganic halide perovskites are explored for various optoelectronic devices, such as solar cells, light emitting diodes, photodetectors, and field effect transistors[1–5]. As a flagship of this advance, perovskite solar cells (PSCs) have achieved a remarkable milestone in power conversion efficiency (PCE) from 3.8% to over 26% at the laboratory scale, positioning them as a strong candidate for next-generation photovoltaics[6]. Commercialization of PSCs and other perovskite devices critically depends on the cost-effective and scalable fabrication ability of high-quality perovskite films.

Currently, spin coating is the most common method for depositing perovskite film in laboratories due to its ease of operation, low equipment cost, and good reproducibility[7,8]. However, achieving homogeneous film over a large-size substrate is challenging because of uneven centrifugal force, leading to substantial waste (>90 %) of the precursor ink[9,10]. For large-area film coating, several industrial processing techniques like blade coating, slot-die coating, and spray coating have been studied[11–15]. Despite offering good scalability and module performance[16–19], they have limitations, including unportable equipment, cumbersome alignment/calibration steps, durative labor maintenance, poor substrate compatibility for some of them, and non-uniform deposition caused by the easy aggregation of perovskite colloidal particles.

Fabrication of perovskite solar modules (PSMs) involves scribing steps, referred to as P1, P2 and P3 scribing, aimed at dividing a large-area device into small-area sub-cells and establishing electrical interconnection in series[20]. These scribes are typically conducted using lasers and/or mask plates[21], demanding high-cost facilities and precise lithography design. The process also requires substantial optimization of laser conditions, including wavelength, power, repetition rate,

[1]Henan Key Laboratory of Quantum Materials and Quantum Energy, School of Quantum Information Future Technology, Henan University, Zhengzhou, PR China. [2]Department of Chemistry, Department of Electrical & Computer Engineering, University of Victoria, Victoria, British Columbia, Canada. [3]These authors contributed equally: Yuhao Song, Miaosen Yao. ✉e-mail: phydongchen@163.com; msaidaminov@uvic.ca; frtan@henu.edu.cn
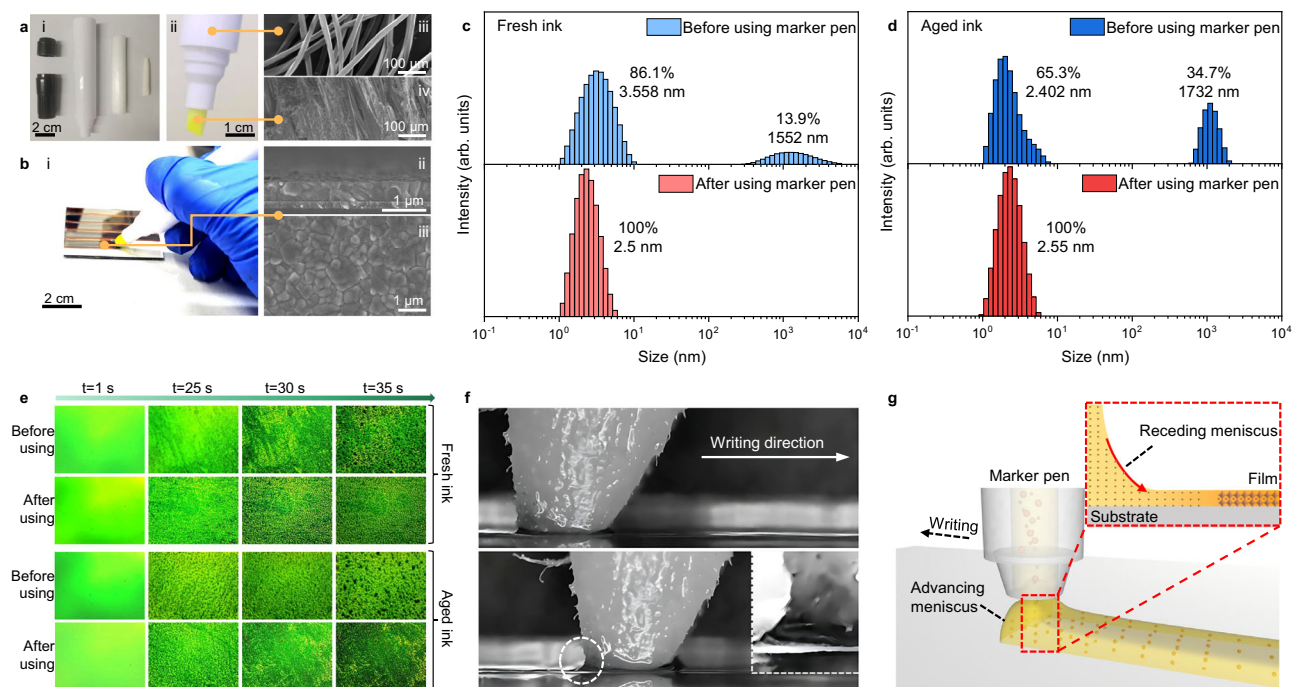
Fig. 1 | Marker pen writing of perovskite films. a (i, ii) Photo of marker pen and scanning electron microscopy (SEM) image of (iii) its core and (iv) tip. **b** (i) Photo capturing the process of handwriting MAPbI₃ perovskite films on a rigid substrate and (ii, iii) SEM images of the resultant perovskite film. **c**, **d** Dynamic light scattering (DLS) particle size analysis in fresh and aged precursor inks before and after using marker pens. **e** In situ microscopy photographs of nucleation evolution of fresh and aged precursor inks before and after using marker pens. **f** In-situ microscopy images of writing dynamics. **g** Schematic diagram of working principle of the MPW method.

scribing speed, and overlap between pulses[22,23]. Moreover, perovskites, in contrast to many photovoltaic materials, exhibit heightened thermal sensitivity, leading to partial degradation or redeposition at the vicinity of the laser scribe[24].

Alternative module fabrication approaches involve depositing each layer's patterning on desired areas, which eliminates scribing steps. Techniques such as screen printing, 3D printing, inkjet printing, spray coating, and roll-to-roll coating have been explored for this purpose[25–29]. However, these methods present limitations, including ink system constraints in screen printing, material incompatibility in 3D printing, uniformity in inkjet printing, material wastage in spray coating, and alignment and substrate compatibility in roll-to-roll coating[30]. In contrast, solution-based pen-writing or pen-drawing is a reliable, convenient, affordable, and self-patternable fabrication method on various substrates. Currently, different types of pens including pencils, ballpoint pens, fountain pens, brush pens, and marker pens, have been employed as film fabrication tools[31–34]. Among them, marker pens have balanced characteristics in large-area deposition and continuous solution supply, offering an opportunity for scalable and uniform processing of self-patterned PSM devices. Marker pen writing (MPW) has been applied in fabricating photodetectors[35], displays[36], electrothermal[37], and energy storage devices[38].

Herein, we introduce this method to fabricate PSCs and fully write perovskite photovoltaic modules, and demonstrate that the MPW can not only self-homogenize perovskite colloidal particles and deposit uniform films with controllable thickness and area, but also self-pattern PSMs on diverse substrates. Using this approach, we achieve efficient and stable low- and room-temperature carbon-electrode PSCs (C-PSCs) on rigid and flexible substrates. Furthermore, the rigid and flexible carbon-electrode PSMs (C-PSMs) with efficiencies of 16.3% and 14.5%, respectively, both written in a mask- and laser-free manner, showcase the large-area self-patterning capabilities of this method. These written C-PSMs can serve as deformable and lightweight power sources for portable and/or wearable electronic products. Irregular C-PSM, such as perovskite solar leaf, showcasing an attempt to blend

technology and art, as well as practical ITO-free PSMs on paper and elastomers, can also be produced by this method.

Results

Marker pen writing of perovskite films

The MPW process for fabricating perovskite film is schematically illustrated in Supplementary Fig. 1. A marker pen is typically composed of three parts: a pen tip, a reservoir core, and a penholder (part i in Fig. 1a), wherein the pen tip is inserted and soaked in the ink reservoir. The reservoir core of the marker pen consists of micron-sized fibers and loose channels (part iii in Fig. 1a), allowing it to spontaneously absorb and uniformly supply ink akin to a sponge through capillary action[39], as evidenced by photoluminescence (PL) images and microscopy photographs (Supplementary Fig. 2). In contrast, the tip of the marker pen is dense and usually crafted by bonding filaments like felt, nylon, bristles, and fibrils[40], enabling continuous, uniform and on-demand delivery of perovskite ink onto the substrate for writing (part iv in Fig. 1a). We found that the tip can serve as a colloidal homogenizer supplying highly monodisperse 2.5 nm particles for both fresh and aged perovskite inks, while preventing delivery of agglomerated 1000+ nm particles (Fig. 1c, d). This characteristic is beneficial for homogeneous nucleation of perovskite crystals (Fig. 1e), and prolongs the use/storage lifespan of precursor ink, as evidenced by the good environmental durability (Supplementary Fig. 3) and reliable manufacturability of MPW (Supplementary Fig. 4).

To reveal the underlying working mechanism of the MPW, we monitored the writing process in situ through optical microscopy. When the pen tip was brought into contact with the substrate and pressed against it, the precursor solution in the reservoir core was continuously released onto the substrate through surface tension and capillary action. During the writing process, the pen tip produced a shear force on the precursor solution due to the relative movement, which induced the formation of menisci at both the advancing and receding sides of the pen head (Fig. 1f). After horizontal movement of a steady-state meniscus at constant speed and pressure (Supplementary
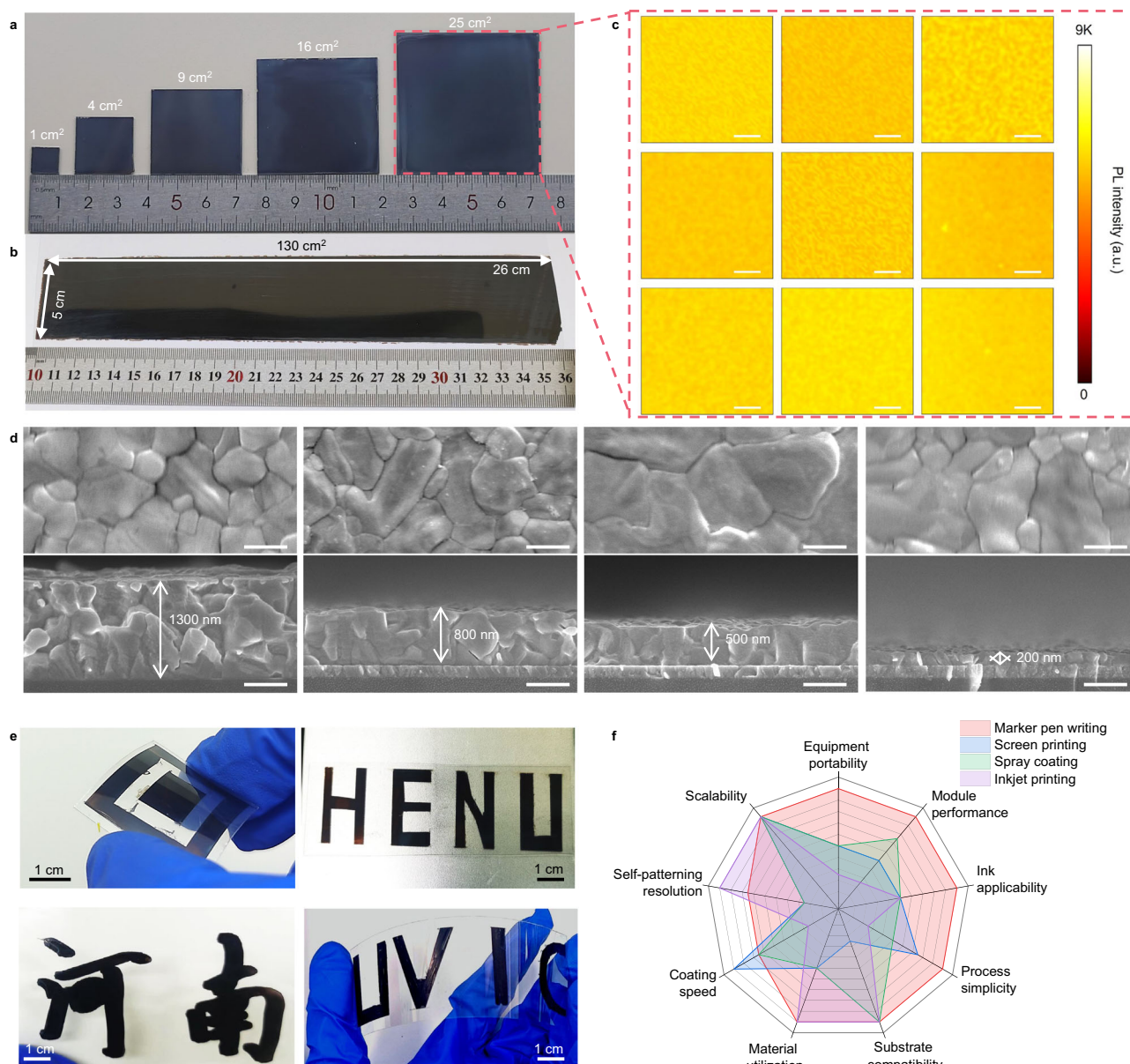
Fig. 2 | Large-area and pattern engineering of perovskite films by MPW.
a Photographs of the handwritten perovskite films of different areas (1–25 cm²).
b Photograph of a 130 cm² handwritten perovskite film. **c** PL mapping of 9 parts of a handwritten 5 cm × 5 cm perovskite film. The scale bar represents a length of 100 μm. **d** Top-view and cross-section SEM images of handwritten perovskite films with different thicknesses obtained by adjusting ink concentration. The scale bar represents a length of 500 μm. **e** Patterned perovskite films written on flexible ITO/ PET substrates, constituting square, square ring, HENU (stands for Henan University), UVIC (stands for University of Victoria), and Chinese characters.
f Comparison of solution-based fabrication methods for patternable perovskite films (more details in Supplementary Table 1).

Fig. 5), the solution filtered by pen tip spread along the substrate, along with the continuous supply of ink (Supplementary Fig. 6), thereby writing a homogeneous wet film (Fig. 1g and Supplementary Fig. 7). After writing precursor film, gas quenching was employed to extract the volatile solvent of 2-methoxy ethanol (2-ME), but left behind high-boiling n-methyl pyrrolidone (NMP) to form an intermediate film; and final annealing led to formation of compact perovskite films with large grains (parts ii and iii in Fig. 1b), meeting the prerequisite for performing PSCs[41,42]. We note that a moderate force strength (~1.5 N) and a fast-drawing speed (~80 mm/s) by mechanical or manual control were optimal to write a homogenous film with a narrow edge (Supplementary Figs. 5 and 8). In addition, the composition of the written perovskite film can be tailored by the ink formulation (Supplementary Fig. 9).

Large-area and patternable perovskite films

One advantage of the MPW method is that it can produce patterned films. Perovskite thin films of the same thickness were deposited on different areas in a single round by adjusting the width of the marker pen tip (Fig. 2a and Supplementary Figs. 10–11). By continuous writing over long lengths, large-sized films with areas of 100+ cm² can be obtained (Fig. 2b). This allows for fabrication of both perovskite small-area and large-area devices.

To assess the uniformity of the written film over a large area, we handwrote a 5 cm×5 cm perovskite film, divided it into 9 parts, and measured the PL mapping of each (Fig. 2c). The PL emission of those 9 parts was spatially uniform, implying good homogeneity of written perovskite film over a large area[43]. This was also validated by UV-vis absorption and steady-state PL of these individual parts, with
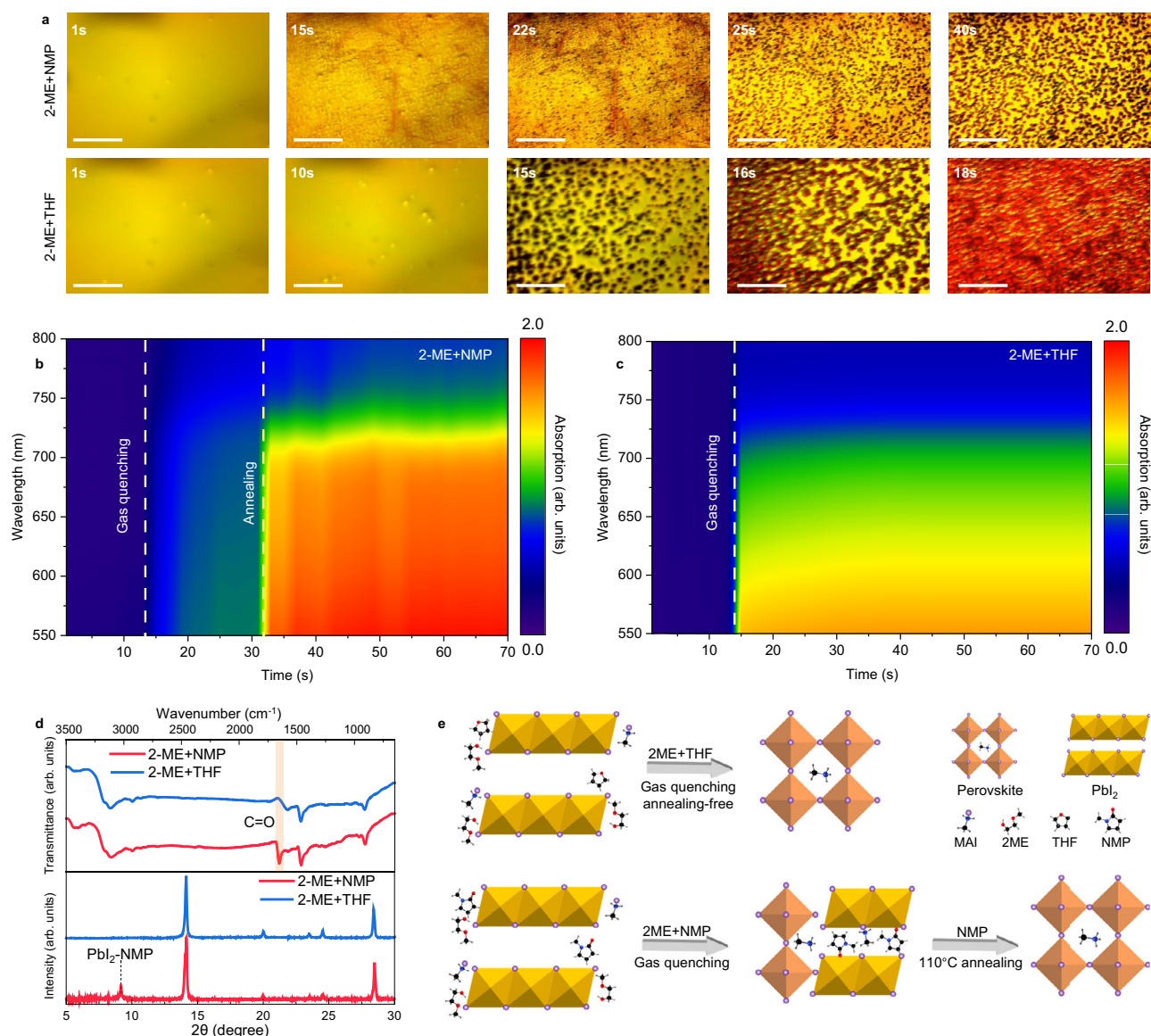
Fig. 3 | Annealed and unannealed perovskite films by MPW. a In situ microscopy photographs of evolution of the perovskite precursor ink during natural drying process. The scale bar represents a length of 10 μm. **b**, **c** Time-resolved in-situ absorption of annealed and unannealed perovskite films. **d** FTIR spectra and XRD patterns of annealing-free perovskite films written using different precursor solvents. **e** Schematic diagram of perovskite crystallization processes using different precursor solvents.

absorption edge at 750 nm and PL peak intensity both showing a variation of only 15% and less (Supplementary Fig. 12). Such good uniformity of large perovskite films is attributed to homogenous colloidal particles and precursor wetting process by the marker pen, as also evidenced by the uniform optical and PL images (Supplementary Fig. 13).

The thickness of the perovskite films by MPW can be customized by controlling the pressure force, writing speed, and concentration of perovskite ink (Fig. 2d and Supplementary Figs. 14–15). Additionally, owing to the freedom and flexibility inherent to marker pens, this method can also realize complex patterns with arbitrary shapes on various substrates (Fig. 2e and Supplementary Fig. 16).

We also compared the MPW approach with the mainstream methods for fabricating patternable perovskite films (Fig. 2f and Supplementary Table 1). Traditional screen printing and spray coating can pattern perovskite film at a high speed of 80+ mm/s via stencil masking; and inkjet printing allows for the mask-free formation of fine patterns at high resolution of less than 50 μm. Unfortunately, they require specialized equipment, frequent maintenance, and cumbersome calibration steps as well as strict control of ink properties. By comparison, the MPW can easily tackle these challenges, making it widely accessible.

Ambient writing of perovskite films

As-coated perovskites are typically annealed to form crystalline films. To probe the practicality of the MPW, we explored the direct writing of perovskite films without annealing step. We replaced high-boiling NMP in the pristine solvent mixture (NMP and 2-ME) with high vapor pressure solvent, tetrahydrofuran (THF), to facilitate rapid solvent drying and crystallization at room temperature, only with gas quenching alone. Figure 3a compares optical microscopy images of the crystallization process of different precursor inks during natural drying. A few small nuclei appeared at ~22 s after using the pristine precursor ink (2-ME + NMP), whereas many large nuclei formed earlier (at ~15 s) and grew rapidly into a uniform and dense film with the volatile precursor ink (2-ME + THF). We then applied in situ UV-Vis absorption
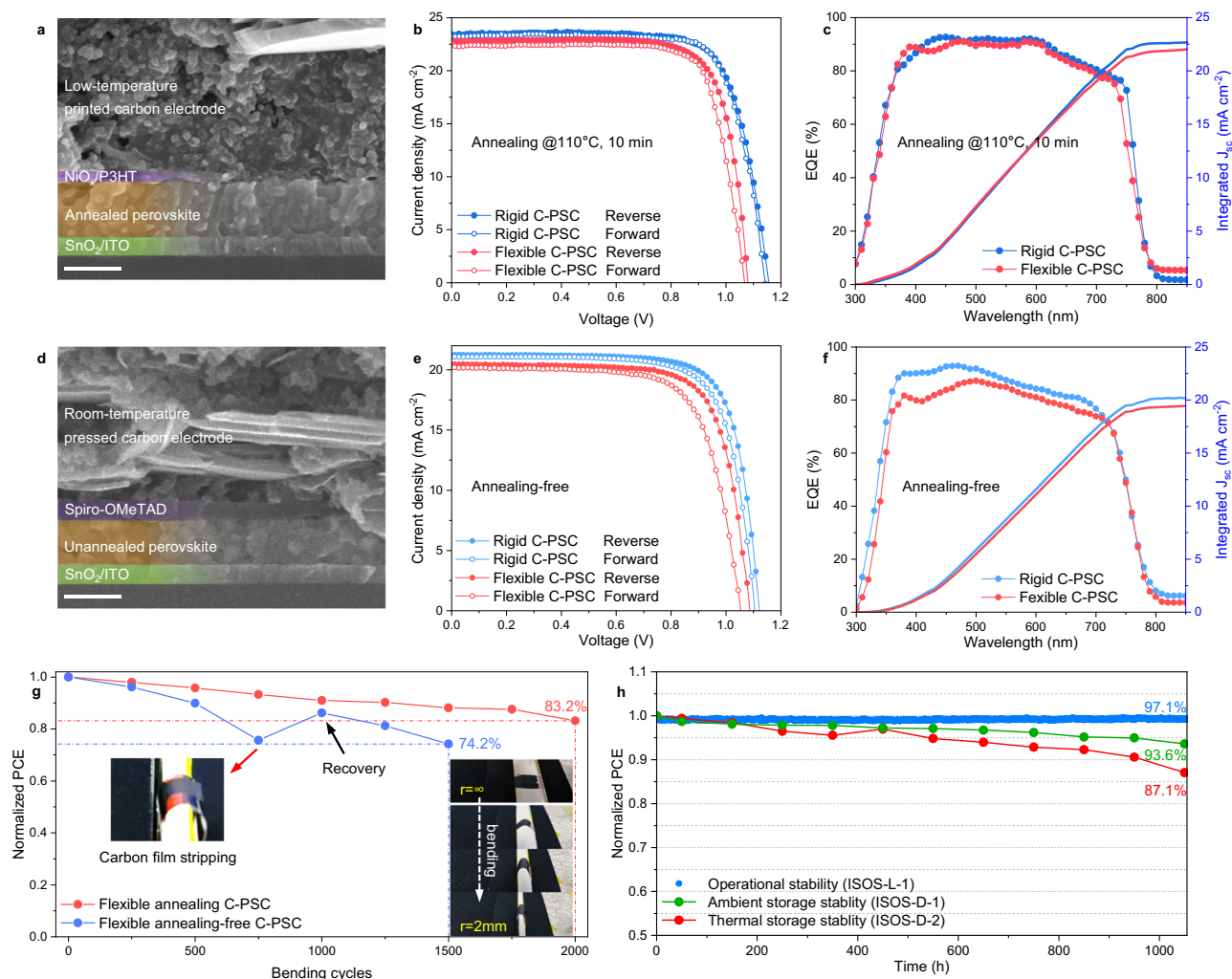
Fig. 4 | Performance of carbon-electrode perovskite solar cells (C-PSCs) by MPW. a Cross-sectional SEM image of low-temperature C-PSC. The scale bar represents a length of 500 nm. **b** Champion J-V curves of the annealed rigid and flexible C-PSCs (perovskite layers made by MPW and annealed at 110 °C for 10 min). **c** External quantum efficiency (EQE) spectra and integrated J_{sc} of the annealed C-PSCs. **d** Cross-sectional SEM image of room-temperature processed C-PSC. The scale bar represents a length of 500 nm. **e** Champion J-V curves of the annealing-free rigid and flexible C-PSCs (perovskite layers made by MPW and dried with gas blowing, without annealing). **f** EQE spectra and integrated J_{sc} of the annealing-free C-PSCs. **g** Efficiency evolution of flexible annealing and annealing-free C-PSCs as a function of mechanical bending cycles at a curvature radius of 2 mm. **h** Long-term ambient, thermal, and operational stabilities of the C-PSCs.

spectroscopy to study the phase transition process for both conditions (Fig. 3b, c). As-written perovskite films showed no absorption features in the 550–800 nm range. When gas quenching was introduced at -13 s, the written precursor films underwent phase transition as evidenced by the appearance of perovskite absorption features. However, due to the strong coordinating of NMP into perovskite in the pristine precursor ink[44], this film did not convert into a perovskite phase until thermal annealing was applied. In contrast, gas quenching rapidly crystallized perovskite at room temperature from volatile perovskite ink (2-ME + THF). This result was further verified by X-ray diffraction (XRD) and Fourier transform infrared (FTIR) spectra in Fig. 3d. The diffraction peak of PbI$_2$·NMP complex (2θ = 9.0°) and FTIR peak of C=O vibration (≈1655 cm^{-1}) disappeared after replacing NMP with THF[45], indicating that the pure-phase perovskite film can be obtained under annealing-free conditions when using 2-ME and THF solvents (Fig. 3e).

We then compared the quality of written perovskite films under annealing and annealing-free conditions (Supplementary Fig. 17). Annealing led to a significant increase in the grain size and charge carrier lifetime. Nevertheless, we also observed a smooth surface, uniform thickness, and densely packed film morphology for the written annealing-free perovskite film, which is promising for fabrication

of PSCs and modules on materials that cannot withstand high temperature[46].

Marker pen written C-PSCs

Having studied the quality of perovskite films made by MPW, we proceeded to construct C-PSCs, with the planar stack architectures of ITO/SnO$_2$/annealed perovskite/P3HT/NiO$_x$/carbon and ITO/SnO$_2$/unannealed perovskite/spiro-OMeTAD/carbon, where both annealed and unannealed perovskite films were handwritten by marker pen. The carbon electrode was prepared by blade-coating carbon paste and curing at 110 °C for 30 min, or directly pressing carbon film at room temperature for the annealing-free device. Figure 4a, d show the cross-sectional SEM images of these C-PSCs, from which the intimate layer-to-layer contacts can be observed in both devices.

Under AM 1.5 G 100 mW/cm^2 illumination, the rigid annealed C-PSC achieved a champion PCE of 20.4% with a short-circuit current density (J_{SC}) of 23.33 mA/cm^2, an open-circuit voltage (V_{OC}) of 1.16 V, and a fill factor (FF) of 75.4% (Fig. 4b, Supplementary Table 2), comparable with the reported best-performing low-temperature spin-coated C-PSCs with a PCE of 20.8%[47]. Corresponding pen-written device with thermally evaporated metal-electrode exhibited a high PCE

of 23.6% (Supplementary Fig. 18). Notably, the flexible annealed C-PSC also attained a high efficiency of 19.0% with a J_{SC} of 22.8 mA/cm^2, a V_{OC} of 1.08 V, and an FF of 77.2%, setting a PCE record for flexible C-PSCs (Supplementary Table 3). Rigid and flexible annealing-free C-PSCs achieved PCEs of 18.0% and 16.4%, respectively, which surpass most reported annealing-free PSCs with metal electrodes (Fig. 4e and Supplementary Table 4). The performance gap between annealed and unannealed C-PSCs is largely due to the change in perovskite film quality upon annealing, as discussed above. Corresponding EQE spectra and integrated J_{SC} values aligned well with the J_{SC} values extracted from J–V measurements within 5% deviation (Fig. 4c, f). In addition, the decrease in EQE after 600 nm is mainly because the black carbon electrode does not back-reflect unabsorbed light (Supplementary Fig. 19).

To probe the reproducibility of our proposed method, we fabricated 20 independent devices for each architecture based by handwriting perovskite films (Supplementary Fig. 20): the efficiency distributions of $19.2 \pm 0.6\%$ and $18.0 \pm 0.5\%$ for rigid and flexible annealed cells, respectively ($16.7 \pm 0.6\%$ and $15.0 \pm 0.7\%$ for rigid and flexible annealing-free devices, respectively), indicate that the MPW is a reproducible method. This reproducibility was further improved with the aid of mechanical control (Supplementary Fig. 21).

We then assessed the mechanical reliability of flexible annealing and annealing-free C-PSCs through bending cycles over a 2 mm radius (Fig. 4g). The annealed device retained 83.2% of its initial efficiency after 2000 bending cycles. By contrast, the annealing-free C-PSCs retained only 75.6% of original efficiency after 750 bending cycles due to the detachment of carbon electrode (insert in Fig. 4g); however, after pressing the carbon film again, the performance of the flexible annealing-free device recovered to 86.2% and remained at 74.2% after 2000 bending cycles.

We also tracked ambient, thermal, and operational stability of our C-PSCs using ISOS-D-1, ISOS-D-2, and ISOS-L-1 protocols[48], respectively (Fig. 4h). The device retained 93.6% of its initial PCE after ~1050 h storage in ambient air without encapsulation; 87.1% after continuous heating at 85 °C with encapsulation; and 97.1% after continuous operation at maximum power point (MPP) under light illumination with encapsulation.

Marker pen written C-PSMs and their applications

Inspired by the pattern engineering ability of the MPW, we proceeded to draw strip sub-cells for the construction of carbon-electrode PSMs (C-PSMs), aiming to eliminate P2 laser scribing step. The P2 etching process is widely recognized as the most critical step for patterning the module layout in series-connected sub-cells. This step must be aggressive enough to completely remove the perovskite and charge transporting layers, and gentle enough, at the same time, to prevent ITO damage[22,49,50]. Additionally, the P2 laser scribing can easily damage the adjacent perovskite layer and flexible polymer substrates, negatively affecting module performance, stability, and reproducibility[51]. In contrast, the MPW method eliminates the need for P2 laser scribing, as it can deposit film in any pattern. The process of fabricating C-PSM by MPW method is schematically illustrated in Fig. 5a, which can be executed step by step manually or mechanically synchronized (Supplementary Fig. 22 and Supplementary Movie 1). The gap between the neighboring perovskite films (namely P2) written by a marker pen depends on the resolution of human's eye (0.1 mm), making it possible to achieve 0.1 mm level (Fig. 5b), thus meeting the architectural requirements of most PSMs[52-54]. To avoid undesired shunting PSMs when layer-by-layer writing, we constructed the staircase layered structure (Supplementary Fig. 23) by gradually reducing the film edge width from the bottom to the top (details are provided in "Methods" section).

We fabricated 4 cm × 4 cm flexible and rigid C-PSMs from 5 single sub-cells connected in series, with each functional layer (excluding carbon electrode) written with marker pens (Fig. 5c). The best-performing rigid and flexible printed C-PSMs showed a PCE of 16.3% (with a J_{sc} of 4.34 mA cm^{-2}, a V_{oc} of 5.5 V, and an FF of 68.1%), and of 14.5% (with a J_{sc} of 4.09 mA cm^{-2}, a V_{oc} of 5.1 V, and an FF of 69.5%), respectively. The module efficiency of 16.3% is much higher than that of traditional screen-printed, spray-coated, and inkjet-printed PSMs (Supplementary Table 1). For perovskite annealing-free conditions, the rigid and flexible room-temperature pressed C-PSMs achieved PCEs of 11.7% and 11.0%, respectively (Supplementary Fig. 24). The V_{oc} of each sub-cell of the rigid/flexible annealing and annealing-free modules reaches >1 V, indicating negligible V_{oc} losses compared to corresponding devices built on a small area. The FF values of the modules are also remarkable given the large sheet resistance of the carbon electrode[55-57].

The MPW method also allows rapid and on-site/-demand fabrication of power supply. To demonstrate the practical applicability of the C-PSMs made by a marker pen, they were utilized as an emergency power supply for outdoor portable electronics, such as an electronic compass and hygrothermograph (Fig. 5d and Supplementary Movie 2). To meet the charging threshold of >3 V for the discharged hygrothermograph, handwriting four sub-cells to construct the rigid C-PSM is sufficient to drive it, continuously providing important data for outdoor use.

The deformable and lightweight nature of flexible marker-written C-PSMs is desirable for wearable electronics, which can be integrated with different functional devices to construct self-powered smart systems[58,59]. As shown in Fig. 5e and Supplementary Movie 3, a smart wristband, as a typical wearable device, can monitor people's physical condition. However, the most important issue with a smart wristband is the low energy source[60]. The flexible C-PSMs written by a marker pen can be attached to the skin, enabling the wristband to work continuously even if there are no batteries or only small capacity batteries are required as backup power. Moreover, when charging the middle-power electronic devices such as mobile phone, several flexible C-PSMs can be connected in series through conductive copper tape. They can maintain high foldability (thickness down to 0.85 mm), bendability (angle up to 360°), and twistability (angle up to 180°), enabling their direct attachment to normal clothing (Fig. 5f and Supplementary Movie 4).

To demonstrate versatility of MPW, we directly handwrote ITO-, carbon-, and annealing-free PSMs with the sub-cell configuration of PH1000/PTAA/perovskite/PCBM/BCP/Ag nanowires (NWs) on both elastic balloons and cellophane paper. As shown in Fig. 5g, h, the PSMs constructed on the spherical surface of a rubber balloon were able to drive an electronic watch even after inflation with a stretch of 7.8% or after deflation with a shrinkage of 7.2% (Supplementary Fig. 25 and Supplementary Movie 5). These PSMs, handwritten on cellophane paper, also exhibited good foldability, which can light an assortment of 0.05 W LEDs after single and even dual folding at 180° (Supplementary Movie 6).

The MPW can also be used to manufacture irregular solar modules, such as biomimetic solar leaves (Fig. 5i and Supplementary Movie 7). The biomimetic solar leaves were constructed by connecting left and right sub-cells in series (Supplementary Fig. 26), where each irregular sub-cell is directly hand-written on the PET-ITO following the structure of SnO_2/perovskite/P3HT/NiO$_x$, and carbon electrodes are pasted on top and interconnected with the bottom ITO of the next cell. These modules can serve not only as a power supply to light an assortment of 0.05 W LEDs, but also be attached to a tree branch with less land requirement and more pleasing aesthetics.

In conclusion, we demonstrated marker pen writing of perovskite solar cells and modules. By using marker pens, not only colloidal sizes can be homogenized and stabilized, but also the films' thickness and area can be tuned from one hundred nanometers to one micrometer and from 1 cm^2 to 100+ cm^2, respectively, meeting
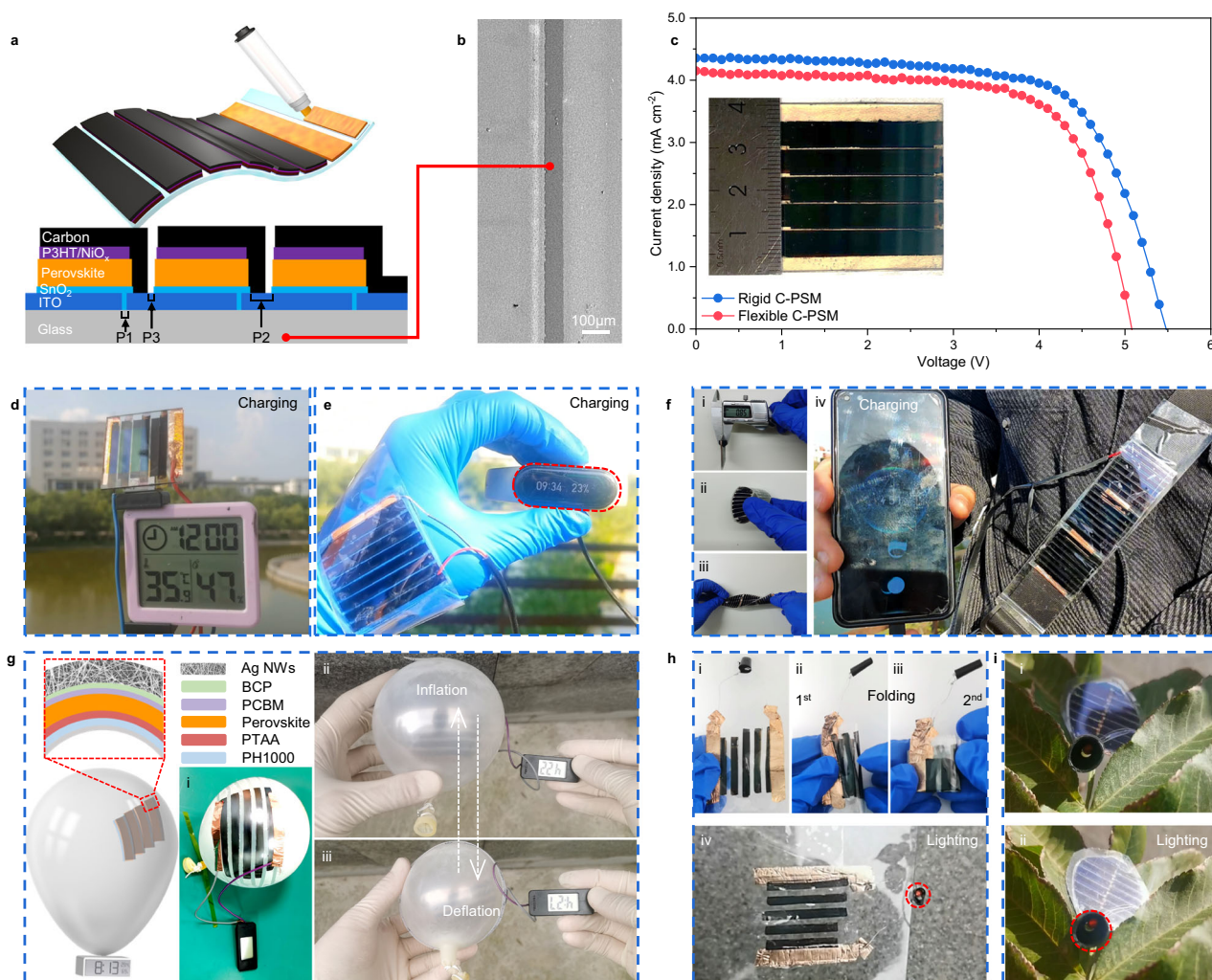
Fig. 5 | Performance and applications of carbon-electrode perovskite solar modules (C-PSMs) by MPW. a Schematic of preparing C-PSM by MPW and module architecture. **b** Minimized distance (P2) between perovskite films written by marker pen. **c** Champion J-V curves of rigid and flexible annealed 4 cm × 4 cm C-PSMs (inset: photograph of the rigid C-PSM). **d** Demonstration of handwritten C-PSMs as power sources to drive the hygrothermograph. **e** Demonstration of flexible C-PSMs as wearable power sources to charge a smart wristband. **f** Demonstration of (i) foldability, (ii) bendability, (iii) twistability of flexible C-PSMs, and (iv) their application as wearable power sources for a mobile phone. **g** Demonstration of handwritten ITO- and annealing-free PSMs on (i) rubber balloons, with the sub-cell configuration of PH1000/PTAA/perovskite/PCBM/BCP/Ag nanowires (NWs), and their application as power sources for an electronic watch under (ii) inflation and (iii) deflation conditions. **h** Demonstration of handwritten ITO- and annealing-free PSMs on (i) cellophane paper, (ii, iii) their foldability, and (iv) their application as power sources for a light-emitting diode (LED). **i** Biomimetic solar leaf handwritten by marker pen and its practical application as the power source for an LED under (i) tree shade and (ii) illumination conditions.

the requirements for the active layer in diverse perovskite photovoltaic devices. An ambient writing of annealing-free perovskite film is also demonstrated by engineering precursor solvent mixture, promoting practicality of this method. The rigid and flexible written C-PSCs exhibit the champion efficiencies of 20.4% and 19.0% under annealing conditions, respectively; 18.0% and 16.4% under annealing-free conditions, respectively. Additionally, inspired by the ambidextrous writing and easy patterning of marker pens, we realize the rigid and flexible C-PSMs in a mask- and laser-free manner. Furthermore, this technology offers a convenient and rapid route for manufacturing of lightweight and deformable power sources, which have been proven to drive portable and/or wearable electronic products like hygrothermographs, smart wristbands, and mobile phones. ITO- and annealing-free PSMs on elastomers and paper, as well as irregular modules of biomimetic solar leaves with balanced art and technology, can also be handwritten with marker pens. The marker pen writing is of low cost, easy patterning, large area, and suitable for on-demand deposition, making it possible to

bring perovskite photovoltaics to more scenarios and enter households.

Methods

Materials

All materials were used as received without further purification. SnO_2 (15% in H_2O colloidal dispersion) was purchased from Alfa Aesar. PbI_2 (99.99%), MAI (99.99%), MABr (99.99%), P3HT (98%), spiro-OMeTAD (99.9%), Li-TFSI (99%), FK209 (98%), tBP (96%), PTAA ($M_n \approx$ 6000-15000), bathocuproine (BCP, 99.5%), and $PC_{61}BM$ (99%) were obtained from Xi'an Polymer Light Technology Corp. KCl (99.99%), guanidinium chloride (GACl, 99%), 2-methoxy-ethanol (2-ME, > 99.5%), chlorobenzene (CB, 99%), tetrahydrofuran (THF, 99.5%), and N-methyl pyrrolidone (NMP, 99.9%) were purchased from Aladdin. The NiO_x-nanoparticles (NPs) in IPA (mass ratio 25%, particle size 10-20 nm) were purchased from China Hengna New Materials. Carbon pastes were obtained from Shanghai Mater Win New Materials Co., Ltd. Clevios PH1000 was obtained from Heraeus Electronic Materials. Ag

nanowires (NWs) dispersion (in IPA) was purchased from XFNANO Materials. Marker pens with different tip widths were directly purchased from Flysea Co., Ltd.

Fabrication of C-PSCs with annealing

The structure of rigid and flexible annealing C-PSCs is ITO-glass (ITO-PET)/SnO$_2$/annealed perovskite/P3HT/NiO$_x$/carbon. First, ITO-glass/-PET substrates were cleaned by ultrasonic sonication in detergent solution, deionized water (DI), acetone, and isopropanol for 30 min. The SnO$_2$ dispersion diluted with DI water in a 1: 4 volume ratio, was then spin-coated onto the flexible and rigid ITO substrates at 4000 rpm for 30 s, followed by annealing at 110 °C and 150 °C for 30 min, respectively. For marker pen writing of MAPbBr$_{3-x}$I$_x$ (x = 0 ~ 3) multicolor perovskite films, pure MAPbX$_3$ (X = I and Br) were first prepared by mixing the PbX$_2$ salt and MAX precursor into DMF: DMSO (9: 1 v/v ratio) at a molar ratio of 1:1 and a concentration of 1.2 mol/L. The precursor was then stirred at 60 °C for 2 h. The MAPbBr$_{3-x}$I$_x$ perovskite was then obtained by mixing pure MAPbI$_3$ and MAPbBr$_3$ at different molar ratios. For marker pen writing of annealed perovskite film used for low-temperature printable C-PSCs, precursor ink was formulated by dissolving stoichiometric MAI and PbI$_2$ in 2-ME and NMP (with a volume ratio of 20:1) at a concentration of 1.0 mol/L, together with 20% mol GACl as the additive. The formulated inks were then injected into the empty reservoir core for use. Next, the perovskite ink was written onto the rigid and flexible ITO/SnO$_2$ substrate surfaces following the user's normal way of handwriting or using motor-driven, computer-controlled writing system (Supplementary Fig. 22 and Supplementary Movie 1). For volatile 2-ME/NMP precursor ink, gas-quenching was applied after marker pen writing, where N$_2$ was sprayed on the precursor film for 5–10 s. The gas pressure at the regulator was set to 0.3 MPa. For DMSO/DMF precursor ink, higher-intensity N$_2$ quenching at 0.4 MPa should be performed for a longer time of 30-40 s. Then the intermediate films were annealed at 110 °C for 10 min in air to get the final perovskite phase. For P3HT HTL, 10 mg/mL P3HT CB solution was spin-coated onto the perovskite layer at 3000 rpm for 30 s and heated at 100 °C for 5 min. After that, the NiO$_x$-NPs were deposited by spin-coating at 3000 rpm for 30 s and annealing at 60 °C for 5 min in air. Finally, carbon pastes were blade coated on the prepared film and annealed at 110 °C for 30 min in the air to obtain the low-temperature printable C-PSC devices. The active cell area was defined at 0.04 cm^2 using 3 M tape and was checked by an optical microscope.

Fabrication of C-PSCs without annealing

The structure of rigid and flexible annealing-free C-PSCs is ITO-glass (ITO-PET)/SnO$_2$/unannealed perovskite/spiro-OMeTAD/carbon. For annealing-free perovskite deposition, the 1.0 M precursor ink was formulated by dissolving stoichiometric MAI and PbI$_2$ in 2-ME and THF (with an optimal volume ratio of 10: 1). Next, the perovskite film was directly written on the rigid and flexible substrate by low-intensity (0.1 MPa) gas quenching for only 3–5 s. The effect of THF dosage on the unannealed film quality is provided in Supplementary Fig. 27. For spiro-OMeTAD HTL, a mixed solution of spiro-MeOTAD (78 mg), Li-TFSI (23 μL, 520 mg/mL in acetonitrile), FK209 (12 μL, 300 mg/mL in acetonitrile), and tBP (39 μL) in 1 mL CB was spin-coated at 3000 rpm for 30 s. Finally, commercial carbon paste was blade-coated onto a glass substrate and soaked in ethanol for 10 min to remove residual solvent. The pre-prepared carbon film was directly pressed onto the HTL under a pressure of 0.3 MPa for 15 s to complete the whole device fabrication. The active area of the cells was defined to be 0.04 cm^2 by shadow mask.

Fabrication of ITO-based C-PSMs

The modules were fabricated on the commercial prepatterned 4 cm × 4 cm ITO-glass/-PET substrates. The written C-PSMs have five sub-cells. The ink formulations and post treatments were processed in the same way as the small-area C-PSC above. Each SnO$_2$, perovskite, P3HT, NiO$_x$, and spiro-OMeTAD films were successively written using 5 mm marker pen, with a length of 4 cm and a gap of 1 mm. These lengths and widths were calibrated using a ruler and checked by an optical microscope. To avoid direct contact of perovskite to bottom electrode (ITO or PH1000), and hole transport layer (P3HT/NiO$_x$ or PTAA) to electron transport layer (SnO$_2$ or PCBM/BCP), we constructed the staircase layered structure (Supplementary Fig. 23) by gradually shorting the film boundary width from the bottom to the top, which can be achieved by increasing the speed, decreasing the pressure or reducing the width of pen tip layer by layer. In addition, the interconnections between the top electrode (carbon electrode or Ag NWs) of one cell and the bottom electrode of the next cell, are dead areas and unaffected by edge alignments. The negligible effect of marker pen writing on the underlying layer is also evidenced in Supplementary Fig. 28. To complete the series interconnection between sub-cells, carbon pastes were doctor-bladed across the active and unwritten areas, in which each unwritten area was further divided by 3 M tape to ensure the insulation of sub-electrode units; or carbon electrode films were directly pressed onto the HTL and interconnecting areas to obtain the annealing-free C-PSMs. The low-temperature printable C-PSMs were obtained by annealing at 110 °C for 30 min in the air.

Fabrication of ITO-free PSMs

To fabricate ITO-free PSM on the various substrates, the diluted PH1000 ink was first handwritten onto the surface of inflated rubber balloons or PDMS-coated cellophane paper to separate the bottom electrode and obtain P1 patterns, and air-dried at room temperature for 2-5 min using a hair blower until the solvent was completely evaporated. Next, PTAA (2 mg/mL, in CB), perovskite (annealing-free), PCBM (23 mg/mL, in CB), and BCP (5 mg/mL, in IPA) inks with decreasing film edges were successively handwritten on top of each PH1000 film, followed by gas blowing to form P2. Finally, the AgNWs ink was directly handwritten on the top of the desired active region and the PH1000 surface of the adjacent cell, forming a series-connected ITO-free module.

Characterization

The pressing force during the marker pen writing process was measured using a commercial pressure sensor (IMS-C20A, WAAAX), as shown in Supplementary Fig. 29. The colloidal sizes were obtained from a dynamic light scattering (DLS, Malvern Instruments Corporation, Nano ZS). The surface and cross-sectional morphologies were obtained using a JSM-7001F field-emission SEM. The absorption spectra and PL spectra of the written films were characterized using UV-Vis-NIR spectrophotometer (Cary 5000) and a fluorescence spectrophotometer (FLS 980, Edinburgh), respectively. The PL mapping image was collected using a HORIBA LabRAM Odyssey system. FTIR spectra were recorded using an INVENIOS FTIR spectrometer (Bruker). AFM was conducted with a Dimension Icon AFM (Bruker). The crystal structures of the written films were examined using D8 Advance X-ray diffractometer (XRD). The current density-voltage (J-V) curves were carried out using a Keithley 2400 Source Measure Unit with a Solar Simulator (Newport, Class 3 A) under 100 mW cm^{-2} illumination (AM 1.5 G) in ambient air (room temperature, humidity of 30–60%). The devices were scanned from 1.2 to -0.1 V and back, with a scan speed of 50 mV/s and a dwell time of 50 ms. The light intensity was calibrated by a standard silicon cell (Newport 91150V-KG5), which was certified by National Renewable and Energy Laboratory (NREL) in 2011. External quantum efficiency (EQE) spectra of the written device were measured using a Crown Technology EQE measurement system (Test Station 500ADX, USA).

Stability test

The ambient stability test of the unencapsulated device was performed following the ISOS-D-1 protocol, involving dark storage in ambient air

(room temperature, humidity of 30–60%). The thermal stability of the encapsulated device was assessed with the ISOS-D-2 test conducted at 85 °C in dark and ambient air. The operational stability test of the encapsulated cell was carried out by applying the ISOS-L-1 protocol under MPPT tracking and simulated AM 1.5 G illumination (LED solar simulator, Tianjin Meitong Intelligent Technology Co., Ltd.) with an intensity of 100 mW cm^{-2} in ambient air. The written C-PSC was encapsulated using cover glass slip and hot melt film sealing.

Reporting summary

Further information on research design is available in the Nature Portfolio Reporting Summary linked to this article.

Data availability

The data supporting the findings of this study are provided in the paper and its Supplementary Information/Source Data file. Any other information can be requested from the corresponding author. Source data are provided with this paper.

References

1. Sun, J. et al. Organic/inorganic metal halide perovskite optoelectronic devices beyond solar cells. *Adv. Sci.* **5**, 1700780 (2018).
2. Younis, A. et al. Halide perovskites: a new era of solution-processed electronics. *Adv. Mater.* **33**, 2005000 (2021).
3. Bing, J. et al. Perovskite solar cells for building integrated photovoltaics-glazing applications. *Joule* **6**, 1446–1474 (2022).
4. Zhao, Y. & Zhu, K. Organic-inorganic hybrid lead halide perovskites for optoelectronic and electronic applications. *Chem. Soc. Rev.* **45**, 655–689 (2016).
5. Wu, S., Chen, Z., Yip, H. L. & Jen, A. K. Y. The evolution and future of metal halide perovskite-based optoelectronic devices. *Matter* **4**, 3814–3834 (2021).
6. Green, M. A. et al. Solar cell efficiency tables (version 62). *Prog. Photovolt: Res. Appl.* **31**, 651–663 (2023).
7. Dai, Z. et al. Interfacial toughening with self-assembled monolayers enhances perovskite solar cell reliability. *Science* **372**, 618–622 (2021).
8. Shi, P. et al. Oriented nucleation in formamidinium perovskite for photovoltaics. *Nature* **620**, 323–327 (2023).
9. Ye, F. et al. Soft-cover deposition of scaling-up uniform perovskite thin films for high cost-performance solar cells. *Energy Environ. Sci.* **9**, 2295–2301 (2016).
10. Xiao, Y. et al. Large-area blade-coated solar cells: advances and perspectives. *Adv. Energy Mater.* **11**, 2100378 (2021).
11. Parida, B. et al. Recent developments in upscalable printing techniques for perovskite solar cells. *Adv. Sci.* **9**, 2200308 (2022).
12. Huang, F., Li, M., Siffalovic, P., Cao, G. & Tian, J. From scalable solution fabrication of perovskite films towards commercialization of solar cells. *Energy Environ. Sci.* **12**, 518–549 (2019).
13. Yang, F. et al. Upscaling solution-processed perovskite photovoltaics. *Adv. Energy Mater.* **11**, 2101973 (2021).
14. Ma, Y. & Zhao, Q. A strategic review on processing routes towards scalable fabrication of perovskite solar cells. *J. Energy Chem.* **64**, 538–560 (2022).
15. Bu, T. et al. Modulating crystal growth of formamidinium-caesium perovskites for over 200 cm^2 photovoltaic sub-modules. *Nat. Energy* **7**, 528–536 (2022).
16. Fei, C. et al. Lead-chelating hole-transport layers for efficient and stable perovskite minimodules. *Science* **380**, 823–829 (2023).
17. Yoo, J. W. et al. Efficient perovskite solar mini-modules fabricated via bar-coating using 2-methoxyethanol-based formamidinium lead tri-iodide precursor solution. *Joule* **5**, 2420–2436 (2021).
18. Yang, F. et al. Fully solution processed pure α-phase formamidinium lead iodide perovskite solar cells for scalable production in ambient condition. *Adv. Energy Mater.* **10**, 2001869 (2020).
19. Chen, S. et al. Stabilizing perovskite-substrate interfaces for high-performance perovskite modules. *Science* **373**, 902–907 (2021).
20. Park, N. G. & Zhu, K. Scalable fabrication and coating methods for perovskite solar cells and solar modules. *Nat. Rev. Mater.* **5**, 333–350 (2020).
21. Palma, A. L. Laser-processed perovskite solar cells and modules. *Sol. RRL* **4**, 1900432 (2020).
22. Brooks, K. G. & Nazeeruddin, M. K. Laser processing methods for perovskite solar cells and modules. *Adv. Energy Mater.* **11**, 2101149 (2021).
23. Faheem, M. B. et al. Insights from scalable fabrication to operational stability and industrial opportunities for perovskite solar cells and modules. *Cell Rep. Phys. Sci.* **3**, 100827 (2022).
24. Li, Z. et al. Scalable fabrication of perovskite solar cells. *Nat. Rev. Mater.* **3**, 18017 (2018).
25. Chen, C. et al. Perovskite solar cells based on screen-printed thin films. *Nature* **612**, 266–271 (2022).
26. Razza, S., Castro-Hermosa, S., Di Carlo, A. & Brown, T. M. Research Update: Large-area deposition, coating, printing, and processing techniques for the upscaling of perovskite solar cell technology. *APL Mater.* **4**, 091508 (2016).
27. Søndergaard, R., Hösel, M., Angmo, D., Larsen-Olsen, T. T. & Krebs, F. C. Roll-to-roll fabrication of polymer solar cells. *Mater. Today* **15**, 36–49 (2012).
28. Bishop, J. E., Smith, J. A. & Lidzey, D. G. Development of spray-coated perovskite solar cells. *ACS Appl. Mater. Interfaces* **12**, 48237–48245 (2020).
29. Saravanapavanantham, M., Mwaura, J. & Bulović, V. Printed organic photovoltaic modules on transferable ultra-thin substrates as additive power sources. *Small Methods* **7**, 2200940 (2023).
30. Chen, C. et al. Screen-printing technology for scale manufacturing of perovskite solar cells. *Adv. Sci.* **10**, 2303992 (2023).
31. Zhao, J., Lo, L. W., Yu, Z. & Wang, C. Handwriting of perovskite optoelectronic devices on diverse substrates. *Nat. Photon.* **17**, 964–971 (2023).
32. Li, Z. et al. Recent Advances in pen-based writing electronics and their emerging applications. *Adv. Funct. Mater.* **26**, 165–180 (2016).
33. Lee, J. W., Na, S. I. & Kim, S. S. Efficient spin-coating-free planar heterojunction perovskite solar cells fabricated with successive brush-painting. *J. Power Sources* **339**, 33–40 (2017).
34. Heo, S. W., Lee, J. Y., Song, H. J., Ku, J. R. & Moon, D. K. Patternable brush painting process for fabrication of flexible polymer solar cells. *Sol. Energy Mater. Sol. Cells* **95**, 3041–3046 (2011).
35. Zhang, T. et al. Pen-writing high-quality perovskite films and degradable optoelectronic devices. *RSC Adv.* **12**, 3924–3930 (2022).
36. Jeong, S. M. et al. Pen drawing display. *Nat. Commun.* **10**, 4334 (2019).
37. Tian, Y., Dong, M., Wang, X., Zhou, Y. & Qian, J. Fully handwritten flexible electrothermal devices using a whiteboard marker pen with carbon nanoparticle ink. *ACS Appl. Electron. Mater.* **6**, 4288–4296 (2024).
38. Jiang, Q., Kurra, N. & Alshareef, H. N. Marker pen lithography for flexible and curvilinear on-chip energy storage. *Adv. Funct. Mater.* **25**, 4976–4984 (2015).
39. Li, X., Li, Q. & Zhao, C. Zero-order controlled release of water-soluble drugs using a marker pen platform. *ACS Omega* **6**, 13774–13778 (2021).
40. de Oliveira, A. E. F., Pereira, A. C. & Ferreira, L. F. Fully handwritten electrodes on paper substrate using rollerball pen with silver nanoparticle ink, marker pen with carbon nanotube ink and graphite pencil. *Anal. Methods* **14**, 1880–1888 (2022).

41. Saliba, M., Correa-Baena, J. P., Grätzel, M., Hagfeldt, A. & Abate, A. Perovskite solar cells: from the atomic level to film quality and device performance. *Angew. Chem. Int. Ed.* **57**, 2554–2569 (2018).

42. Lee, J. W., Lee, D. K., Jeong, D. N. & Park, N. G. Control of crystal growth toward scalable fabrication of perovskite solar cells. *Adv. Funct. Mater.* **29**, 1807047 (2019).

43. Chen, H. et al. A solvent- and vacuum-free route to large-area perovskite films for efficient solar modules. *Nature* **550**, 92–95 (2017).

44. Chao, L. et al. Solvent engineering of the precursor solution toward large-area production of perovskite solar cells. *Adv. Mater.* **33**, 2005410 (2021).

45. Xie, L., Hwang, H., Kim, M. & Kim, K. Ternary solvent for $CH_3NH_3PbI_3$ perovskite films with uniform domain size. *Phys. Chem. Chem. Phys.* **19**, 1143–1150 (2017).

46. Liu, C., Cheng, Y. B. & Ge, Z. Understanding of perovskite crystal growth and film formation in scalable deposition processes. *Chem. Soc. Rev.* **49**, 1653–1687 (2020).

47. Lu, X. et al. Efficient carbon electrode perovskite solar cells with robust buffer interfaces. *J. Mater. Res. Technol.* **24**, 8162–8170 (2023).

48. Khenkin, M. V. et al. Consensus statement for stability assessment and reporting for perovskite photovoltaics based on ISOS procedures. *Nat. Energy* **5**, 35–49 (2020).

49. Chu, L. et al. High-performance large-area perovskite photovoltaic modules. *Nano Res. Energy* **1**, e9120024 (2022).

50. Castriotta, L. A. et al. Reducing losses in perovskite large area solar technology: laser design optimization for highly efficient modules and minipanels. *Adv. Energy Mater.* **12**, 2103420 (2022).

51. Kosasih, F. U., Rakocevic, L., Aernouts, T., Poortmans, J. & Ducati, C. Electron microscopy characterization of P3 lines and laser scribing-induced perovskite decomposition in perovskite solar modules. *ACS Appl. Mater. Interfaces* **11**, 45646–45655 (2019).

52. Liu, Z. et al. A holistic approach to interface stabilization for efficient perovskite solar modules with over 2000-h operational stability. *Nat. Energy* **5**, 596–604 (2020).

53. Tong, G. et al. Scalable fabrication of >90 cm² perovskite solar modules with >1000 h operational stability based on the intermediate phase strategy. *Adv. Energy Mater.* **11**, 2003712 (2021).

54. Ding, Y. et al. Single-crystalline TiO_2 nanoparticles for stable and efficient perovskite modules. *Nat. Nanotechnol.* **17**, 598–605 (2022).

55. Dong, C. et al. Carbon-based all-inorganic perovskite solar cells: Progress, challenges and strategies toward 20% efficiency. *Mater. Today* **50**, 239–258 (2021).

56. Fagiolari, L. & Bella, F. Carbon-based materials for stable, cheaper and large-scale processable perovskite solar cells. *Energy Environ. Sci.* **12**, 3437–3472 (2019).

57. Bogachuk, D. et al. Perovskite solar cells with carbon-based electrodes - quantification of losses and strategies to overcome them. *Adv. Energy Mater.* **12**, 2103128 (2022).

58. Hu, Y. et al. Flexible perovskite solar cells with high power-per-weight: progress, application, and perspectives. *ACS Energy Lett.* **6**, 2917–2943 (2021).

59. Zhang, J., Zhang, W., Cheng, H. M. & Silva, S. R. P. Critical review of recent progress of flexible perovskite solar cells. *Mater. Today* **39**, 66–88 (2020).

60. Wang, Z., Song, Z., Yan, Y., Liu, S. & Yang, D. Perovskite-a perfect top cell for tandem devices to break the S-Q limit. *Adv. Sci.* **6**, 1801704 (2019).

Acknowledgements

Author contributions

Conceptualization and Methodology: C.D., Y.S. and M.I.S.; Investigation: Y.S., M.Y., G.W., D.Z., Y.D., J.T. and Q.W.; Writing—Original Draft: Y.S. and C.D.; Writing—Review & Editing: C.D., G.Y., Y.G., W.Z., S.D., M.I.S., and F.T.; Supervision: C.D. and M.I.S., Y.S. and M.Y. contributed equally.

Competing interests

The authors declare no competing interests.

Additional information

Supplementary information The online version contains supplementary material available at https://doi.org/10.1038/s41467-025-61459-w.

Correspondence and requests for materials should be addressed to Chen Dong, Makhsud I. Saidaminov or Furui Tan.

Peer review information *Nature Communications* thanks the anonymous, reviewer(s) for their contribution to the peer review of this work. A peer review file is available.

Reprints and permissions information is available at http://www.nature.com/reprints

Publisher's note Springer Nature remains neutral with regard to jurisdictional claims in published maps and institutional affiliations.